Brain-targeted co-delivery of therapeutic gene and peptide by multifunctional nanoparticles in Alzheimer's disease mice

Article *in* Biomaterials · December 2015

DOI: 10.1016/j.biomaterials.2015.11.060

CITATIONS
19

READS
215

10 authors, including:

Yang Liu

68 PUBLICATIONS **2,151** CITATIONS

SEE PROFILE

Jianfeng Li

Fudan University

34 PUBLICATIONS **1,445** CITATIONS

SEE PROFILE

Xi He

University of Wisconsin–Madison

23 PUBLICATIONS **363** CITATIONS

SEE PROFILE

Bin Ji

National Institute of Radiological Sciences

66 PUBLICATIONS **1,322** CITATIONS

SEE PROFILE

Biomaterials 80 (2016) 33–45

Contents lists available at ScienceDirect

Biomaterials

journal homepage: www.elsevier.com/locate/biomaterials

Brain-targeted co-delivery of therapeutic gene and peptide by multifunctional nanoparticles in Alzheimer's disease mice

Yang Liu [a], Sai An [a], Jianfeng Li [a], Yuyang Kuang [a], Xi He [a], Yubo Guo [a], Haojun Ma [a], Yu Zhang [a], Bin Ji [c], Chen Jiang [a, b, *]

[a] Key Laboratory of Smart Drug Delivery, Ministry of Education, Department of Pharmaceutics, School of Pharmacy, Fudan University, 826 Zhangheng Road, Shanghai, 201203, PR China
[b] State Key Laboratory of Medical Neurobiology, Fudan University, Shanghai, 201203, PR China
[c] Molecular Imaging Center, National Institute of Radiological Sciences, Chiba, Japan

ARTICLE INFO

Article history:
Received 25 August 2015
Received in revised form
24 November 2015
Accepted 29 November 2015
Available online 2 December 2015

Keywords:
Brain-targeted delivery
Gene therapy
Alzheimer's disease
Aβ
Tau-fibril
Non-coding RNA

ABSTRACT

Multifunctional nanocarriers are increasingly promising for disease treatment aimed to regulate multiple pathological dysfunctions and overcome barriers in drug delivery. Here we develop a multifunctional nanocarrier for Alzheimer's disease (AD) treatment by achieving therapeutic gene and peptide co-delivery to brain based on PEGylated dendrigraft poly-L-lysines (DGLs) *via* systemic administration. The dendritic amine-rich structure of DGLs provides plenty reaction sites and positive charge for drug loading. Successful co-delivery of drugs overcoming the blood–brain barrier by brain-targeted ligand modification was demonstrated both *in vitro* and *in vivo*. The pharmacodynamics study of the system following multiple-dosing treatment was verified in transgenic AD mice. Down-regulation of the key enzyme in amyloid-β formation was achieved by delivering non-coding RNA plasmid. Simultaneous delivery of the therapeutic peptide into brain leads to reduction of neurofibrillary tangles. Meanwhile, memory loss rescue in AD mice was also observed. Taken together, the multifunctional nanocarrier provides an excellent drug co-delivery platform for brain diseases.

1. Introduction

The nano-scaled drug-loading particles (known as nanoparticles) have been successfully applied for delivering varieties of imaging and therapeutic molecules for disease diagnosis and therapy in the recent two decades [1–3]. However, it remains challenging to develop therapeutic nanoparticles for brain diseases such as Alzheimer's disease (AD) [4,5]. On one hand, the complex pathology of brain diseases usually involves more than one pathway dysfunctions [6,7], requiring co-delivery of multiple drugs to achieve the synergetic effects. On the other hand, the blood–brain barrier (BBB) is believed to be one of the most compact structures in the body as it serves as a guard to protect the brain from extraneous substances invasion [8]. Thus, it makes it extraordinarily difficult for delivering therapeutic agents into the brain through non-invasive systemic administration [9]. The multifunctional nanoparticles provide an effective strategy to solve the above issues. The neurotrophic factors have been successfully delivered into the brain to play their neuron protective role by using multifunctional nanocarriers [10–16]. The incorporation of different therapeutic agents into one formulation can simplify dosing regimens and improve patient compliance [17,18]. The different drug loading modes effectively reduce the interaction among drugs. With the specific ligand modification, the accumulation in targeted sites can be improved while the nonspecific uptake will be reduced. Besides, the polymeric materials with high biocompatibility and degradability as nanocarriers could be applied to multiple dosing administration regimen to ensure sustained long-term therapeutic effects.

The two main pathological hallmarks of AD include extracellular amyloid-beta (Aβ)-containing plaques and intracellular fibrils consisted of phosphorylated-tau (p-tau) [19–21]. Thus, dual target therapy for AD involving both reduction of Aβ plaque deposition and inhibition of p-tau associated fibrils formation will benefit from dual therapeutic mechanisms. Aβ is generated from the amyloid

* Corresponding author. Key Laboratory of Smart Drug Delivery, Ministry of Education, Department of Pharmaceutics, School of Pharmacy, Fudan University, 826 Zhangheng Road, Shanghai, 201203, PR China.
E-mail address: jiangchen@fudan.edu.cn (C. Jiang).

http://dx.doi.org/10.1016/j.biomaterials.2015.11.060
0142-9612/

precursor protein (APP) [22,23]. The conversion from APP to Aβ is through sequential proteolytic cleavages by β-site APP cleaving enzyme 1 (BACE1), being identified as a major β-secretase. BACE1 activity has been up-regulated in sporadic AD cases, particularly in neurons around Aβ plaques [24,25]. Down-regulation of BACE1 level could effectively reduce Aβ formation [26,27]. Thus, efficient and specific delivery of therapeutic gene targeting to silence the BACE1 mRNA in brain parenchyma cells is promising to decrease the Aβ burden [28]. However, insufficient BACE1 level may also lead to numerous behavioral and physiological deficits such as memory loss and emotional deficits [29,30]. Consequently, the crucial boundaries between the physiology and pathology of BACE1 indicate that its expression must be precisely regulated, allowing the enzyme to perform its physiological functions while avoiding serious consequences of over- or under-expression [31]. The BACE1 antisense (BACE1-AS) is a natural antisense transcript non-coding RNA that regulates BACE1 expression. The reduction of Aβ by BACE1-AS knockdown with specific siRNA has been demonstrated previously *via* 14-day continuous pump-mediated infusion [31]. Herein, we aim to achieve the BACE1-AS down-regulation through the less invasive intravenous administration by delivering the BACE1-AS shRNA encoding plasmids (pshBACE1-AS), which are more stable in circulation than siRNA [32].

On the other hand, the inhibition of tau-related fibril formation in AD brain provides another effective strategy to prevent or delay the progress of AD [33]. Due to abnormal phosphorylation and conformational changes, tau tends to aggregate into fibrils [34]. A highly specific peptide inhibitor of fibril formation is designed and developed by computer-aided, structure-based design [35]. This all-D amino-acid inhibitor (sequence: D-TLKIVW, named as D-peptide) has been shown to disrupt the p-tau associated fibril formation in AD. If this therapeutic D-peptide can be delivered to the brain, the formation of p-tau containing fibril will be greatly inhibited.

In this study, we focused on the evaluation of multifunctional drug delivery nanoparticles for therapeutic gene and peptide drug co-delivery across the BBB targeting two key pathological pathways in AD. A 29 amino-acid peptide derived from rabies virus glycoprotein (named as RVG29) was applied as the brain-targeted modification. It was found to bind the specific n-acetylcholine receptors, which were widely expressed in BBB and brain parenchyma cells [36]. We successfully observed the gene expression in brain with the RVG29 modified gene delivery nanoparticles after intravenously administration previously [37]. The dendrigraft poly-L-lysines (DGLs) were synthetic polymers with dendritic structures consisted of L-lysine monomers [38]. The rich amine groups of the DGLs offered plenty of modification sites and positive charge under physiological pH. Furthermore, the high biocompatibility and degradability of DGLs allowed multiple dosing administration regimens [39]. It was important to ensure the sustained down-regulation of BACE1 level and persistent inhibition of fibril formation to achieve prompt intervention of AD pathology at the early stage considering the chronic and long-term progression of AD. Both the brain-targeted RVG29 and D-peptide were modified to DGLs through bi-functional PEG linker (Fig. 1). The resultant DGLs-PEG-RVG29-D-peptide was further complexed with plasmid DNA encoding BACE1-AS shRNA, the therapeutic gene in this study, yielding DGLs-PEG-RVG29-Dpeptide/pshBACE1-AS nanoparticles (NPs). The characteristics of the NPs was investigated. The ability of gene and peptide drugs co-delivery by the NPs was confirmed through fluorescence microscopy, flow cytometry, *in vitro* BBB model, and *in vivo* imaging system. The pharmacodynamics study of the NPs in APP/PS1 double transgenic AD mice model was evaluated by measurement of BACE1 level, Aβ staining, p-tau fibril immunostaining and behavioral tests. The toxicity and *in vivo* immunogenicity were also studied as supportive preclinical safety evidence.

2. Materials and methods

2.1. Materials

Dendrigraft poly-L-lysines (DGLs) (containing 123 lysines, generation 3) were obtained from COLCOM (Montpellier Cedex, France). α-Malemidyl-ω-N-hydroxysuccinimidyl polyethyleneglycol (NHS-PEG-MAL, molecular weight (MW) = 3500) was purchased from JenKem Technology Co., Ltd (Beijing, China). The two peptides (RVG29 sequence: YTIWMPENPRPGTPCDIFTNSRGKRASNGC and D-amino-acid peptide sequence: D-TLKIVWGKKKC)) were synthesized by Chinese Peptides Co., Ltd (Hangzhou, China). The BODIPY fluorophore (4,4-difluoro-5,7-dimethyl-4-bora-3a, 4a-diaza-s-indacene-3-propionic acid, sulfosuccinimidyl ester, sodium salt), 4,6-diamidino-2-phenylindole (DAPI) and YOYO-3 iodide were purchased from Molecular Probes (Eugene, OR, USA). Near-infrared fluorescence dye IR-783 sulfosuccinimidyl ester was provided by Pro. C. Li (School of Pharmacy, Fudan University). The BACE-1 antibody (BACE (M83)) and phosphorylated tau antibody (p-Tau (Ser 396)) were purchased from Santa Cruz Biotechnology, Inc. Thioflavin-S as well as other chemical agents were purchased from Sigma–Aldrich Co. LLC.

2.2. Plasmids, cell lines and animals

The BACE1-AS shRNA encoding plasmid (pshBACE1-AS) and scramble shRNA encoding plasmid (pshSc) were constructed into pGPU6/Neo plasmid vector by Genepharma Ltd. Co. The sense strand of BACE1-AS shRNA sequence was 5′-caccTAGAAGGGTCTAAGTGCAGACATCTTGGCtcaagagGCCAAGATGTCTGCACTTAGACCCTTCTAttttttg-3'. Uppercase letters indicated 29-nucleotide (nt) BACE-1 AS target sequences and lowercase letters indicated hairpin sequences necessary for the directional cloning into the plasmid vector. Scramble shRNA encoding plasmid used as negative control had random sequences (sense strand 5′-caccGTTCTCCGAACGTGTCACGTcaagagattacgtgACACGTTCGGAGAAttttttg-3′) with no homology. The plasmid DNA (pDNA) grown in E. coli was isolated using the Endo-Free Plasmid Mega Kit (Qiagen GmbH, Germany).

Brain capillary endothelial cells (BCECs) were kindly provided by Prof. J. N. Lou (the Clinical Medicine Research Institute of the Chinese-Japanese Friendship Hospital). Primary BCECs were cultured as described previously [40]. Cells used in this study were between passage 10 and passage 20. The SH-SY5Y cell line was kindly provided by Prof. L. Y. Feng (Shanghai Institute of Materia Medica, Chinese Academy of Sciences). All cells were cultured at 37 °C under a humidified atmosphere containing 5% CO_2.

Nude mice (4–5 week old) of 20–25 g body weight and C57BL/6J mice were purchased from the Department of Experimental Animals, School of Pharmacy, Fudan University. Double transgenic (Tg) mice ((APPswe, PSEN1dE9)85Dbo/Mmjax) with C57BL/6J background expressing a chimeric mouse/human amyloid precursor protein (Mo/HuAPP695swe) and a mutant presenilin 1 (PS1-dE9) were obtained from Model Animal Research Center of Nanjing University, and used as AD model animal. All the animals were maintained under standard housing conditions. Animal experiments in this study were carried out in accordance with guidelines evaluated and approved by the ethics committee of Fudan University to ensure the humane animal care and use. Mice were housed in a clean room with one mice per cage. Mice were given access to water ad libitum and exposed to a 12:12 h light–dark cycle at 25 ± 1 °C. The experimental methods were optimized to

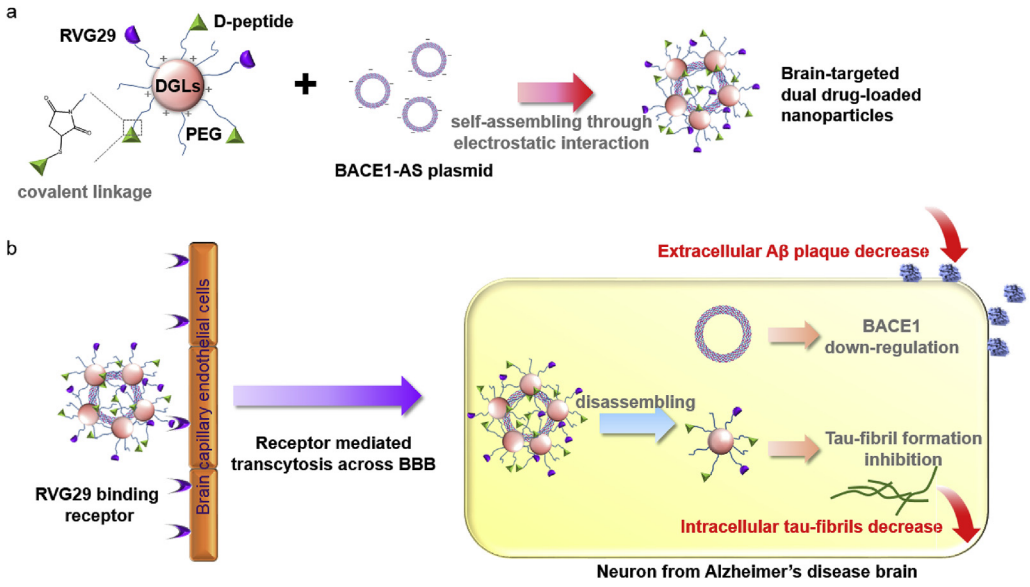

Fig. 1. Schematic design of therapeutic gene and peptide co-delivery system based on DGLs. (a) Two modes of drug loading using brain-targeted DGLs vector. The therapeutic peptide was covalently linked to DGLs, while therapeutic plasmid was encapsulated by DGLs through electrostatic interactions, yielding DGLs-PEG-RVG29-D-peptide/pshBACE1-AS NPs. (b) After intravenous administration, the DGLs-PEG-RVG29-D-peptide/DNA NPs were able to cross the BBB by RVG29 binding receptor-mediated transcytosis. The NPs were further uptaken by diseased neurons of AD in the brain through endocytosis. Upon endosomal escape, the released therapeutic gene (pBACE1-AS) downregulated BACE1 expression, resulting in a reduction of extracellular Aβ plaques. Simultaneously, the D-peptides inhibited tau-fibril formation, leading to a decrease in the intracellular tau-fibrils.

avoid discomfort, distress or pain to the mice. The appropriate analgesics and/or anesthetics were used when necessary. When mice were killed because of experimental endpoints or ethical reasons, mice were sacrificed by carbon dioxide asphyxiation followed by cervical dislocation. These procedures were selected because they did not interfere with post necropsy analysis.

2.3. Preparation and characterization of NPs

DGLs-PEG-RVG29-D-peptide was freshly synthesized (seen in Supporting Information) and diluted to appropriate concentrations in PBS (pH 7.4). DNA solution (100 μg DNA/ml 50 mM sodium sulfate solution) was added to obtain specified weight ratio (6:1, DGLs to DNA, w/w) and immediately vortexed for 30 s at room temperature. Freshly prepared NPs were used in the following experiments. YOYO-3-labeled DNA was prepared according to the recommended protocols. The YOYO-3-labeled DNA was used in preparation of fluorescent NPs for cellular uptake analysis. The morphology of the DGLs-PEG-RVG29-D-peptide/DNA NPs as well as DGLs-PEG-RVG29/DNA NPs was observed by transmission electron microscopy (TEM, JEM-2010/INCA OXFORD) after the samples were stained with 5 μL of 1% phosphotungstic acid aqueous solution (Sigma–Aldrich, USA) for 3 min. The particle size and zeta-potential of the NPs were measured by Zetasizer Nano (Malven, England).

2.4. The transcytosis across the in vitro BBB model

To investigate whether the DGLs-PEG-RVG29-D-peptide/DNA NPs could cross the BBB, the transportation study was done using *in vitro* BBB model. The procedure of BCECs monolayer formation was mentioned previously [40]. DGLs was iodinated with radioactivity of 1 mCi ^{125}I/mg DGLs using the Bolton–Hunter reagents. Radiolabeled DGLs were applied to synthesize DGLs-PEG-RVG29-D-peptide as well as DGLs-PEG-RVG29. 250 μl FBS-free medium was added to the donor chamber at time 0. At the same time, BCECs monolayer was treated with DGLs-PEG-RVG29-D-peptide/DNA NPs and DGLs-PEG-RVG29/DNA NPs, respectively, with a final amount of 20 μg DGLs/100 μl. The incubation was performed at 37 °C on a rocking platform at 50 rpm. The radioactivity of ^{125}I in each aliquot was assessed using a γ-counter. The apparent permeability (P_{app}) was calculated as described in Supporting Information.

2.5. Cellular uptake evaluation

The therapeutic peptide was firstly reacted with fluorescence dye BODIPY (excitation wavelength = 492 nm/emission wavelength = 515 nm) in PBS (pH = 8.0) at room temperature for 2 h. Meanwhile therapeutic plasmid was labeled with YOYO-3 (excitation wavelength = 612 nm/emission wavelength = 632 nm). Unreacted dye was removed through dialysis with membrane molecular weight cut-off (MWCO) at 10,000 Da. Compared with rich amine groups in DGLs and plenty charged density of plasmids, the fluorescence labeling would not affect the size and surface charge of NPs significantly given the fixed complex ratio of DGLs and plasmids. The SH-SY5Y cells were seeded at a density of 2×10^4 cells/well in 24-well plates (Corning-Coaster, Tokyo, Japan) and checked under the microscope for similar confluency and morphology. After that, SH-SY5Y cells were treated with BODIPY-labeled DGLs-PEG-RVG29-D-peptide/DNA NPs loading YOYO-3-labeled DNA at the concentration of 30 μg/150 μl measured by DGLs in the PBS (pH7.4) for 1 h at 37 °C. Then, cells were washed with PBS (pH7.4) for three times and observed by fluorescence microscope (Leica, Germany). In case of flow cytometry analysis, SH-SY5Y cells were seeded at a density of 8×10^4 cells/well in 6-well plates (Corning-Coaster, Tokyo, Japan) and incubated for similar confluency and morphology. SH-SY5Y cells were incubated with BODIPY-labeled DGLs-PEG-RVG29-D-peptide/DNA NPs loading YOYO-3-labeled DNA for 1 h. After that, the cells were washed three times with phosphate buffer solution (PBS, pH 7.4), trypsinized and centrifuged at 1200 rpm for 5 min to remove dead cell segments and obtain a cell pellet, which was subsequently re-suspended in PBS (pH 7.4) and analyzed using a flow cytometer (BD, USA). The fluorescence signals of BODIPY and YOYO-3 were collected using corresponding channels. For each sample, 10,000

events were collected and analyzed. SH-SY5Y cells cultured under the normal conditions served as the control. The mean fluorescence intensity was compared quantitatively between non-targeted DGLs-PEG-D-peptide/DNA NPs and brain-targeted DGLs-PEG-RVG29-D-peptide/DNA NPs.

2.6. In vivo imaging study

To minimum the imaging interference from auto-fluorescence of the animals, D-amino-acid was labeled with near-infrared dye IR-783 (excitation wavelength = 766 nm/emission wavelength = 798 nm) instead of BODIPY. The non-targeted DGLs-PEG-D-peptide/DNA NPs and brain-targeted DGLs-PEG-RVG29-D-peptide/DNA NPs loading YOYO-3-labeled DNA were injected through the tail vein of nude mice (3 mice in each group), respectively, at dose of 50 μg DNA/mouse which was determined based on our previous research. Images were taken by IVIS Spectrum *in vivo* imaging system (Cailper, PerkinElemer, USA) 1 h after intravenous injection when mice were anesthetized. Then, the mice were sacrificed by injection of chloral hydrate *via* tail vein. The principal organs (including brain, heart, kidney, liver, lung, and spleen) were removed. The *ex vivo* distribution of NPs was compared by IVIS Spectrum *in vivo* imaging system.

2.7. Treatment regimen in AD mice

AD mice were maintained for about 9-month-old. Animals were weighed every three days to indicate basic status. At the 30th week after birth, 30 mice were randomly divided into five groups (6 mice in each group) and administrated intravenously with saline, DGLs-PEG-RVG29/pshSc NPs (equivalent 300 μg DGLs, 50 μg pshSc), DGLs-PEG-RVG29/pshBACE1-AS NPs (equivalent 300 μg DGLs, 50 μg pshBACE1-AS), DGLs-PEG-RVG29-D-peptide/pshSc NPs (equivalent 300 μg DGLs, 50 μg pshSc) and DGLs-PEG-RVG29-D-peptide/pshBACE1-AS NPs (equivalent 300 μg DGLs, 50 μg pshBACE1-AS), respectively once a week until the 34th week after birth. The concentration of DNA used was 1 mg/ml (50 μl used). The equivalent DGLs concentration in each group was diluted to 3 mg/ml (100 μl used). As a result, the total volume for one single injection was 150 μl. The regimen was shown in Supporting Information.

2.8. Real-time quantitative RT-PCR analysis

For quantitative assessment of RNA levels, total RNA from substantia nigra area in different groups was prepared using Trizol LS reagent (Invitrogen, USA) following manufacturer instructions. The RT-PCR analysis was done by Shanghai GenePharma Co. Ltd. Values obtained were normalized to the amount of GAPDH. The primer and reverse primer: BACE-1: 5′ GACAACCTGAGGGGAAAGTCCG, 5′ GTCCACCAGGATGTTGAGCGTC; BACE1-AS: 5′ GACTGTCACTGACCGAGGAGGC, 5′ CAACTACGACAAGAGCATTGTGGAC; GAPDH: 5′ GATGACATCAAGAAGGTGGTGA, 5′ ACCCTGTTGCTGTAGCCATATTC. Briefly, 5 μl of template RNA were denatured (95 °C/3 min). Reactions were performed using 50 nM primer. Amplifications were done in a Stratagene MX3000P Real-time PCR machine (Stratagene, US) with the following cycle parameters: 45 min at 42 °C (reverse transcription), 10 min at 85 °C (RT inactivation and PCR polymerase activation), 40 cycles of 95 °C/12 s, and 62 °C/60 s.

2.9. Determination of BACE-1 level

Mice with different NPs administration were sacrificed on the 34th week. The BACE1 level was determined by semi-quantitatively western blot and qualitatively by immunofluorescence (detailed methods seen in Supporting Information).

2.10. Amyloid plaques deposition evaluation

Thioflavine S could stain amyloid specifically, taking on an apple green color under the fluorescence microscope. The 1% thioflavine S aqueous solution was freshly prepared. Coronal brain sections were obtained as previously mentioned [37]. Briefly, brains were removed, fixed in 4% paraformaldehyde for 48 h, placed in 15% sucrose PBS solution until subsidence (6 h), then in 30% sucrose until subsidence (24 h). After this, brains were frozen in OCT embedding medium (Sakura, Torrance, CA, USA) at 80 °C. Frozen sections of 20 μm thickness were prepared with a cryotome Cryostat (Leica, CM 1900, Wetzlar, Germany). To proceed the staining, firstly, sections were hydrated to distilled water. The sections were incubated with 1% $K_2S_2O_5$/1% oxalic acid solution for 5 min following the incubation with 0.25%$KMnO_4$ for 5 min. Then, the section was rinsed in distilled water. After that, thioflavine S solution was placed for 8 min. Subsequently, the sections were differentiated in 70% alcohol for 5 min. Representative images were taken using a microscope (DMI 4000B, Leica, Germany).

2.11. Evaluation of tau level in brain

Coronal brain sections were obtained as previously mentioned [37] and processed for phosphorylated tau antibody immunofluorescence staining using phosphorylated tau antibody (p-Tau (Ser 396)) (1:50; Santa Cruz Biotechnology, USA). Alexa Fluor 488 conjugated goat anti-rabbit secondary antibody (1:1000; CST, USA) was used for fluorescence microscope (DMI 4000B, Leica, Germany) observation. For quantitative analysis of the percentage of p-tau positive signals, coronal section images were counted using software Image-Pro Plus Version 6.0.

2.12. Morris water maze test

At 30 week of age, six AD mice of each group were evaluated spatial learning and memory abilities by the Morris water maze test. The Morris water maze (ANY-maze, Stoelting, U.S.A) apparatus was a white circular pool (100 cm diameter and 50 cm height) with four quadrants. The detailed methods were described in Supporting Information. The average data from daily tests were used for statistical analysis. At the end of the training period, the mice were tested on a spatial probe trial in which the platform was removed, and they were allowed to swim freely for 60 s. The time spent to reach the platform initially, ratio of time spent in the target quadrant and the times of crossing the platform were recorded.

2.13. Statistical analysis

The data was presented as means ± SD. The statistical significance was determined using student's t-test and analysis of variance (ANOVA one way) using GraphPad Instat 3 software. After comparing the overall difference between groups, the Tukey's honestly significant difference (HSD) post-hoc test was undertaken to specify where the differences occurred between groups.

3. Results

3.1. Preparation and characterization of DGLs-PEG-RVG29-D-peptide/DNA NPs

NMR spectra of DGLs-PEG-RVG29 and DGLs-PEG-RVG29-D-peptide shown in Fig. S1a, b indicated successful synthesis of DGLs-PEG-RVG29-D-peptide. The average particle sizes of DGLs-PEG-

RVG29/DNA and DGLs-PEG-RVG29-D-peptide/DNA NPs determined by dynamic light scattering (DLS) were about 97 nm and 110 nm with PDI below 0.3, respectively (Fig. 2 and Table S1). The zeta-potential of DGLs-PEG-RVG29/DNA and DGLs-PEG-RVG29-D-peptide/DNA NPs were 6.11 mV ± 4.04 mV and 7.72 mV ± 2.80 mV, respectively. The TEM images of the DGLs-PEG-RVG29-D-peptide/DNA NPs as well as DGLs-PEG-RVG29/DNA NPs showed both of the NPs had spherical morphology (Fig. 2c and d).

The cytotoxicity of DGLs-PEG-RVG29-D-peptide/DNA NPs was evaluated on BCECs by MTT assay (Fig. S2). The cell viability was above 80% at concentrations of DGLs below 200 μg/ml. The result could ensure the integrity of BCECs monolayer as *in vitro* BBB model in the following transcytosis study.

As shown in Fig. 2e, after complexed with DGLs-PEG-RVG29-D-peptide, nearly no free DNA was detected by both electrophoresis (Fig. 2e, lane 3) and quantitative EB exclusive analysis compared with free DNA (Fig. S3). DGLs-PEG-RVG29-D-peptide was able to completely encapsulate the DNA at the weight ratio used in this study. The peptide conjugation reaction efficiency was monitored by determining the free thiol groups using Ellman's reagent. Negligible thiol groups were measured indicating all the peptides were conjugated to the DGLs-PEG after the reaction at the designed ratio. The stability of DNA in NPs were also shown in Fig. 2e after 4 h treatment of 10% serum containing medium. After heparin replacement, the DNA in the NPs was observed to have nearly 90% recovery. The result demonstrated the DNA loading NPs were stable in serum containing environment which mimicked the *in vivo* circulation environment. On the other hand, free DNA after 10% serum treatment, the recovery percentage was much lower which may attribute to the degradation by DNase in the serum.

3.2. The peptide and plasmid DNA co-delivery ability of DGLs-PEG-RVG29-D-peptide/DNA NPs

The DGLs-PEG-RVG29-D-peptide/DNA NPs with BODIPY-labeled DGLs and YOYO-3-labeled DNA were incubated with SH-SY5Y cells. SH-SY5Y cells expressed nicotinic acetylcholine receptors which could bind the RVG29 peptide [41,42] and facilitate

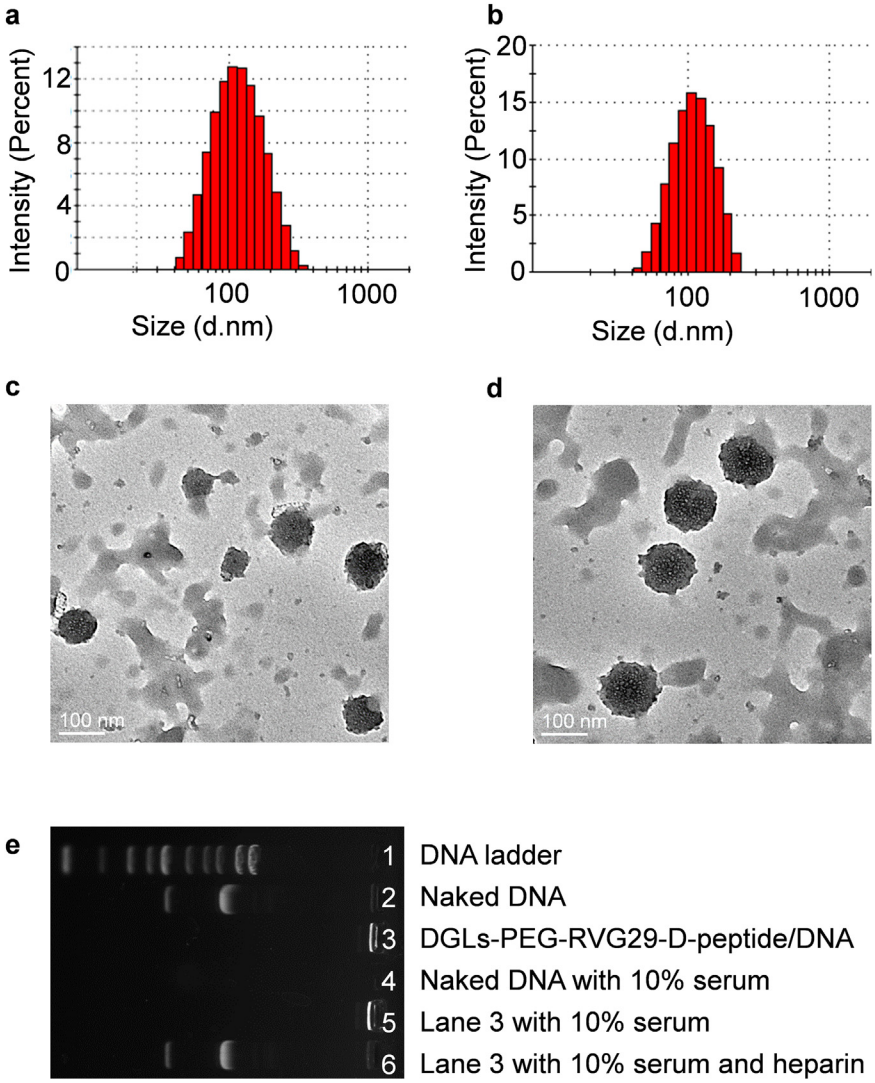

Fig. 2. Characterizations of DGLs-PEG-RVG29-D-peptide/DNA NPs. DLS results of (a) DGLs-PEG-RVG29/DNA and (b) DGLs-PEG-RVG29-D-peptide/DNA NPs. TEM image of (c) DGLs-PEG-RVG29/DNA and (d) DGLs-PEG-RVG29-D-peptide/DNA NPs. (e) DNA encapsulation by DGLs-PEG-RVG29-D-peptide at DGLs/DNA weight ratio 6:1 as evaluated by the gel retardation assay. For stability study, naked DNA with serum or DGLs-PEG-RVG29-D-peptide/DNA with serum, DNA or DGLs-PEG-RVG29-D-peptide/DNA were incubated with 10% serum for 4 h at 37 °C, respectively. For DGLs-PEG-RVG29-D-peptide/DNA with 10% serum and heparin, after incubation with serum, 10 fold excessive heparin was added to replace the DNA from the NPs.

the cellular uptake of targeted NPs more efficiently than non-targeted DGLs-PEG-D-peptide/DNA NPs. The fluorescence microscopy images as well as overlayed images of different fluorescence channels were shown in Fig. 3a–h. The green signal indicated BODIPY-labeled D-peptide, while the red signal indicated YOYO-3-labeled DNA. The co-localized signal of green and red showed yellow.

The above results were further confirmed quantitatively by flow cytometry analysis. The representative flow cytometry results were shown in Fig. 3i and j. The quadrant 1 and 2 (Q1 and Q2) showed the signals of YOYO-3 channel. The quadrant 2 and 4 (Q2 and Q4) showed the signals of BODIPY channel. The quadrant 2 represented the YOYO-3 and BODIPY dual-positive cells. Most of the signals were detected in quadrant 2 indicating the peptide and plasmid DNA were co-delivered into the cells by DGLs-PEG-RVG29-D-peptide/DNA NPs. The mean fluorescence intensity was compared between non-targeted DGLs-PEG-D-peptide/DNA and DGLs-PEG-RVG29-D-peptide/DNA NPs treated cells (Fig. 3). The results showed that the signals of both YOYO-3-labeled DNA and BODIPY-labeled peptide were higher in DGLs-PEG-RVG29-D-peptide/DNA NPs treated cells than that of DGLs-PEG-D-peptide/DNA NPs treated cells.

3.3. The transcytosis transport of DGLs-PEG-RVG29-D-peptide/DNA NPs across the in vitro BBB model

The transport studies of non-targeted DGLs-PEG/DNA, brain-targeted DGLs-PEG-RVG29/DNA, and brain-targeted DGLs-PEG-RVG29-D-peptide/DNA NPs were shown in Fig. 3l. The apparent permeability (P_{app}) of RVG29 modified brain-targeted NPs was

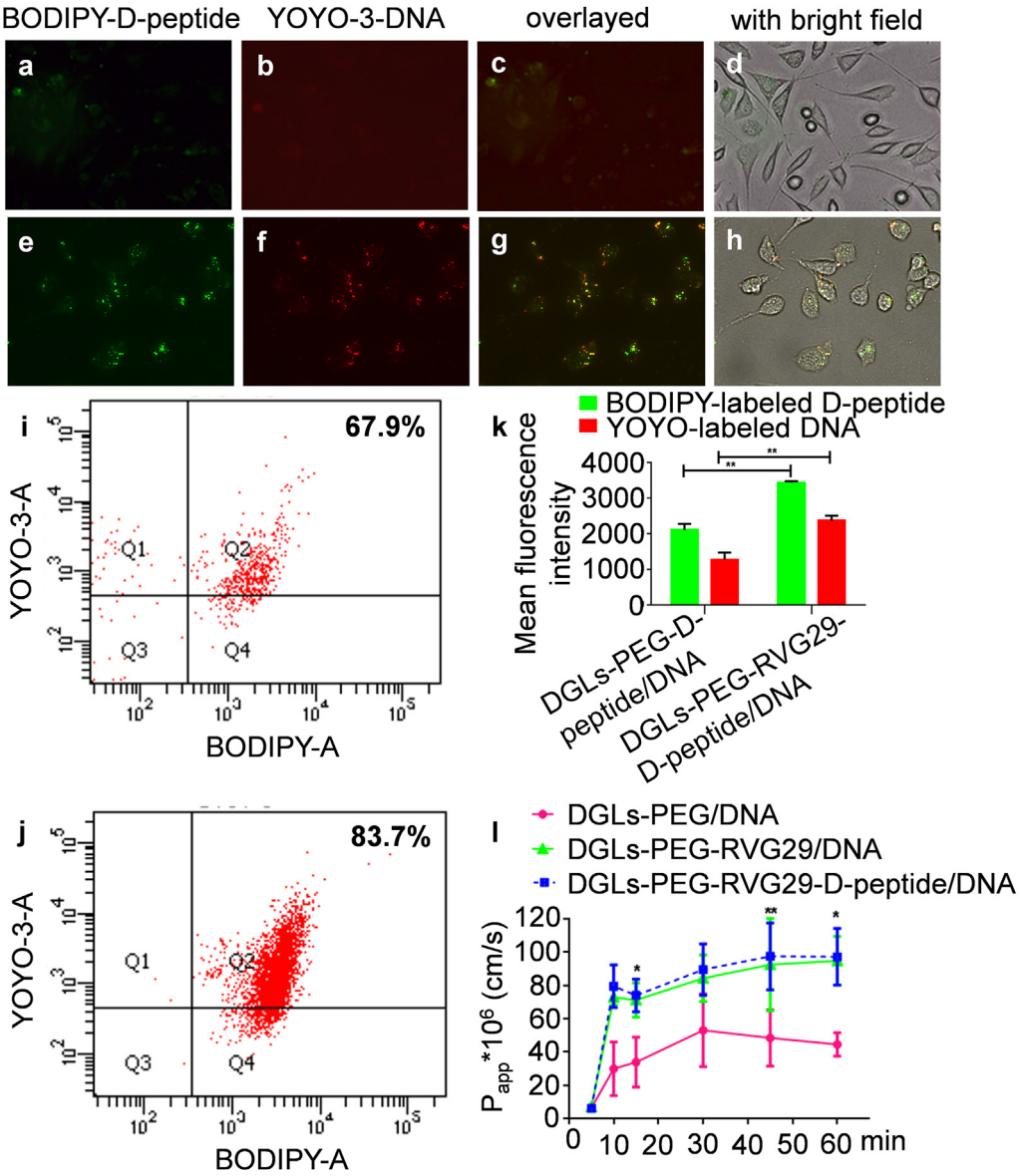

Fig. 3. D-peptide and DNA co-delivery evaluation. (a–d) DGLs-PEG-D-peptide/DNA and (e–h) DGLs-PEG-RVG29-D-peptide/DNA NPs through fluorescence microscopy and flow cytometry. (a, e) Fluorescence image of BODIPY-labeled D-peptide signal. (b, f) Fluorescence image of YOYO-3-labeled DNA signal. (c) Overlayed image of (a) and (b), (g) Overlayed image of (e) and (f), yellow signal was co-localization of green signal and red signal. (d) Overlayed image of (c) and bright field. (h) Overlayed image of (g) and bright field. Magnification × 20 (i) Flow cytometry analysis of DGLs-PEG-D-peptide/DNA NPs. (j) Flow cytometry analysis of DGLs-PEG-RVG29-D-peptide/DNA NPs. (k) Cellular uptake fluorescence intensity comparison of DGLs-PEG-RVG29-D-peptide/DNA NPs and non-targeted DGLs-PEG-D-peptide/DNA NPs. Significance: **$p < 0.01$. (l) The permeability of ^{125}I-labeled NPs across BCECs monolayer. Significance:*, $p < 0.05$; **, $p < 0.01$, significance represents DGLs-PEG-RVG29/DNA or DGLs-PEG-RVG29-D-peptide/DNA NPs vs. DGLs-PEG/DNA NPs. (For interpretation of the references to color in this figure legend, the reader is referred to the web version of this article.)

significantly higher than that of non-targeted NPs since 10 min after NPs incubation with the BCECs monolayer. The brain-targeted NPs showed higher BBB-crossing efficiency than non-targeted NPs in the *in vitro* BBB model. The modification of therapeutic D-peptide did not affect the permeability of the RVG29 modified targeted NPs. Furthermore, the transendothelial electrical resistance (TEER) of the BBB monolayer did not change significantly before and after experiments, verifying the integrity of the BBB model during the incubation.

3.4. *In vivo imaging evaluation of peptide and plasmid DNA co-delivery by DGLs-PEG-RVG29-D-peptide/DNA NPs*

According to NPs transcytosis study by *in vitro* BBB model (Fig. 3l), the transportation rate reached the plaque after 1 h incubation with NPs. The result suggested that the transportation process which was *via* the receptor mediated endocytosis would be saturated within 1h after the NPs exposure. As a result, the *in vivo* imaging figures were taken 1h after the injection. Fig. 4a showed distinct fluorescent signal (in green) from YOYO-3-labeled plasmid DNA accumulated in mice brain and kidney when administrated with the DGLs-PEG-RVG29-D-peptide/DNA NPs intravenously. Meanwhile, the fluorescence in the spleen of the DGLs-PEG-D-peptide/DNA NPs injected mouse was higher while the fluorescence in brain was too weak to be detected. The distribution of two different NPs modified with IR-783-labeled D-peptide (Fig. 4b) exhibited a similar accumulation tendency with that of YOYO-3-labeled plasmid DNA fluorescent signals. The overlay image of YOYO-3 signal and IR-783 signal was shown in Fig. 4c.

The principal organs including brain, heart, liver, spleen, lung and kidney were removed for *ex vivo* imaging analysis (Fig. S4 and Fig. 4d–f). The signals were observed to accumulate in the brain, liver, spleen and kidney in DGLs-PEG-RVG29-D-peptide/DNA NPs treated mice, while the signal in brain was much weaker in DGLs-PEG-D-peptide/DNA NPs treated mice. The co-localization signal (yellow = green plus red) in the brain was more obvious in targeted DGLs-PEG-RVG29-D-peptide/DNA NPs (Fig. 4f, right) treated mice than that of non-targeted NPs treated ones (Fig. 4f, left). A mixture of IR-783-labeled peptide and YOYO-labeled DNA and a mixture of NPs with IR-783-labeled peptide and NPs with YOYO-labeled DNA were used as control. This experiment was replicated to ensure the repeatability of the results. The results (Fig. S5) demonstrated that the DGLs-PEG-RVG29-D-peptide/DNA NPs was able to deliver the D-peptide and DNA to the brain. The brain signals of a mixture of D-peptide and DNA treated group resembled the saline treated group, which indicated neither the free D-peptide nor DNA could get across the BBB entering the brain without delivery carriers.

3.5. *BACE1 mRNA level analysis*

Treatment regimen by DGLs-PEG-RVG29-D-peptide/pshBACE1-AS NPs in AD mice was mentioned previously. BACE1 mRNA levels in hippocampus were quantitatively measured by real-time PCR (RT-PCR) in mice injected with different NPs or negative control after four-dosing regimen (Fig. 5a). The BACE1 mRNA levels in AD mice brain increased compared to non-transgenic normal mice. The BACE1 mRNA levels decreased in AD mice brain treated with NPs loading therapeutic plasmid, which was close to that of non-transgenic normal mice. The administration of NPs loading scramble RNA-encoding plasmid failed to interfere the level of BACE1 mRNA level in AD mice.

3.6. *BACE1 level measurement by western blot*

The BACE1 level was measured by western blot (Fig. 5b). The BACE1 in AD mice hippocampus remained at a lower level after reduplicative injections with NPs loading BACE1-AS-encoding plasmid. The NPs loading scramble RNA-encoding plasmid were again proved to have little effect on the BACE1 level. The down-regulation of BACE1 level was directly caused by the decrease of BACE1 mRNA. Meanwhile, the decrease of BACE1 mRNA was mediated by the change of BACE1-AS RNA level. This evidence suggested successful delivery of therapeutic plasmid by the brain-targeted vector DGLs-PEG-RVG29 with/without the modification of therapeutic D-peptide.

3.7. *BACE1 immunofluorescence in hippocampus*

The BACE1 level was also compared by immunofluorescence assay in AD/normal mice treated with different NPs or saline (Fig. 5c–h). The BACE1 positive signals were lower in DGLs-PEG-RVG29/pshBACE1-AS and DGLs-PEG-RVG29-D-peptide/pshBACE1-AS NPs injected groups compared to other groups. The staining of BACE1 in normal mice was much less than that in AD mice with the

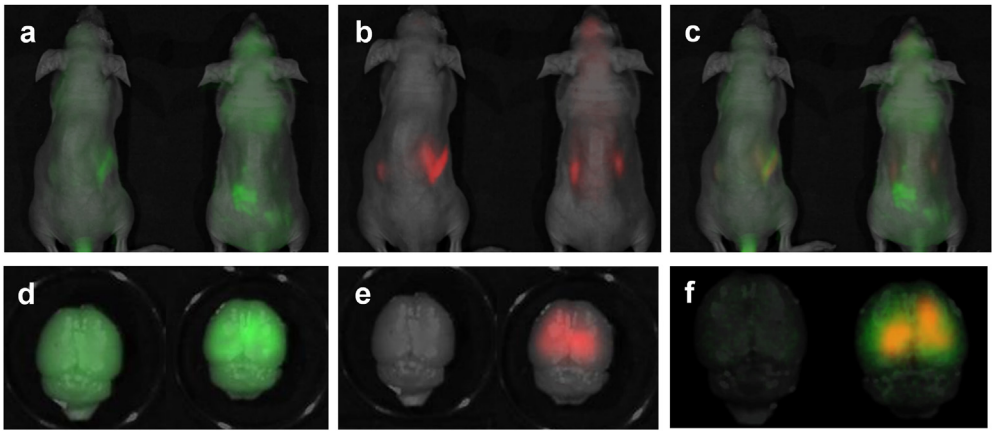

Fig. 4. *In vivo* distribution of NPs after intravenous administration. Images were taken at 1 h after injection. (a) *In vivo* imaging fluorescence signal of YOYO-3-labeled DNA. (b) *In vivo* imaging fluorescence signal of IR-783-labeled D-peptide. Left mouse was injected with DGLs-PEG-D-peptide/DNA NPs while right mouse was injected with DGLs-PEG-RVG29-D-peptide/DNA NPs. (c) Overlayed *in vivo* signal of YOYO-3 and IR-783. (d) *Ex vivo* imaging brain fluorescence signal of YOYO-3-labeled DNA in organs. (e) *Ex vivo* imaging brain fluorescence signal of IR-783-labeled D-peptide in organs. Left brain was from mouse injected with DGLs-PEG-D-peptide/DNA NPs while right brain were from mouse injected with DGLs-PEG-RVG29-D-peptide/DNA NPs. (f) Overlayed signal of YOYO-3 and IR-783 in brain.

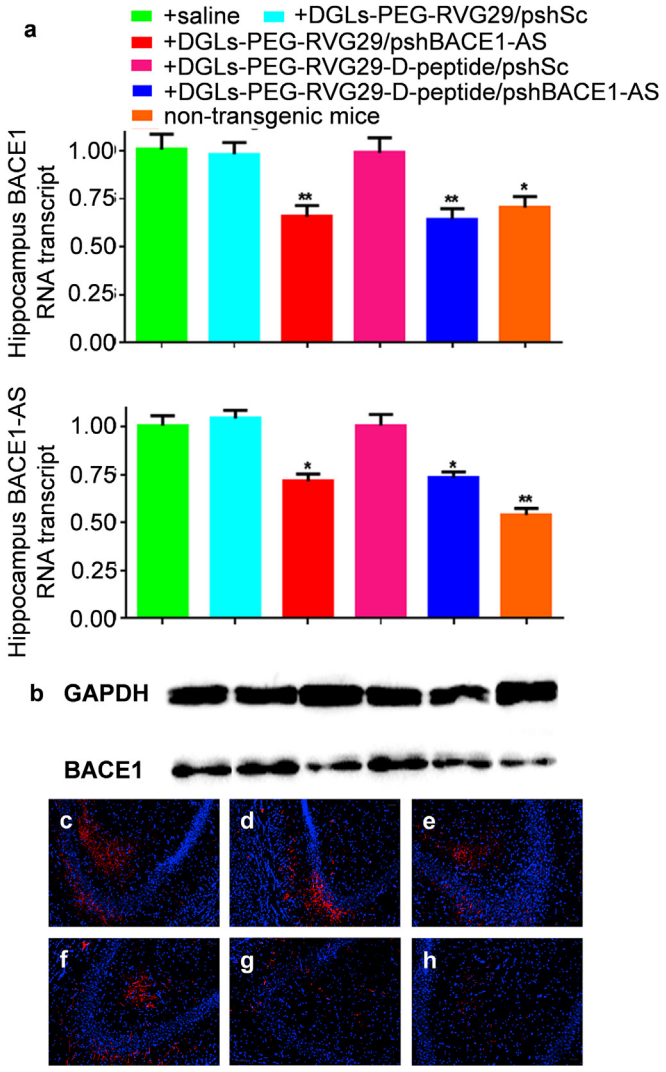

Fig. 5. Evaluation of BACE1 levels in hippocampus region from APP/PS1 transgenic mice and non-transgenic mice with different treatment. (a) RT-PCR analysis of BACE1 mRNA and BACE1-AS levels in APP/PS1 and control mice with different NPs treatment. Data are expressed as means ± S.E.M (n = 3). Significance: *p < 0.05; **p < 0.01, significantly different as compared with saline treated APP/PS1 mice. (b) BACE1 level comparison by western blot in hippocampus of mice with different NPs treatment and control mice. Lane 1 (from left): +saline; lane 2: +DGLs-PEG-RVG29/pshSc; lane 3: +DGLs-PEG-RVG29/pshBACE1-AS; lane 4: +DGL-PEG-RVG29-D-Peptide/pshSc; lane 5: + DGL-PEG-RVG29-D-Peptide/pshBACE1-AS; lane 6: non-treated non-transgenic mice. (c–h) BACE1 positive immunofluorescence at hippocampus in mice with different NPs treatment: (c) +saline; (d) +DGLs-PEG-RVG29/pshSc; (e) +DGLs-PEG-RVG29/pshBACE1-AS; (f) +DGLs-PEG-RVG29-D-peptide/pshSc; (g) +DGLs-PEG-RVG29-D-peptide/pshBACE1-AS; (h) non-treated non-transgenic mice. Magnification × 20.

saline treatment. This result also indicated that the up-regulation of BACE1 level was a significant hallmark in AD pathology.

The above results proved that DGLs-PEG-RVG29/pshBACE1-AS and DGLs-PEG-RVG29-D-peptide/pshBACE1-AS NPs multiple-dosing administration could mediate BACE1-AS RNA reduction, resulting in BACE1 mRNA silencing and downregulation of BACE1 level in hippocampus of AD mice brain.

3.8. Amyloid plaques deposition evaluation

Thioflavine S binded to amyloid specifically, presenting an apple green color under fluorescence microscopy. Thioflavin S-labeled amyloid deposits (green signal) were clearly noticeable in the cortex layer and hippocampus of AD mice with NPs loading scramble plasmid as well as saline treatment (Fig. 6 and Fig. S6). The signal was much less in AD mice treated with NPs loading BACE1-AS shRNA plasmid. Few amyloid deposits were observed in normal mice (Fig. 6f and l). This result was in agreement with the earlier experiment that showed decreased BACE1 level reduced Aβ peptide formation, which lead to the decrease of amyloid deposits. *Tau-positive immunostaining in hippocampus.*

The therapeutic D-peptide possessed binding affinity for p-tau-containing fibrils, allowing it to inhibit the p-tau-associated fibril formation, another characterized pathology in AD. Because p-tau proteins were the main components of fibrils, tau-positive immunostaining was performed to indicate the status of fibrils level in the brain. The tau-positive signals were much higher in AD mice hippocampus treated with NPs without D-peptide modification compared to that treated with NPs with D-peptide modification (Fig. 7a–f). The results demonstrated that D-peptide played a role in disrupting the fibril formation in hippocampus. The immunostaining was presented quantitatively in Fig. 7g.

3.9. The behavioral test results by morris water maze

Morris water maze was used to assess the effect of learning acquisition in AD mice with different NPs treatment. When AD mice were treated with DGLs-PEG-RVG29-D-peptide/pshBACE1-AS NPs *via* intravenous administration according to the regimen, they spent the least time to reach the platform compared with other NPs or saline treated AD mice. The result was slightly longer than that of normal mice. The AD mice groups treated with NPs loaded with single therapeutic component (either therapeutic peptide or therapeutic plasmid) did not perform as well as NPs loaded with dual therapeutic components. The mice treated with DGLs-PEG-RVG29/pshSc NPs behaved similarly with the control AD mice group. The representative swimming paths of mice with different treatment were shown in Fig. 8a. The results were also presented statistically as the percentage of time spent in targeted quadrant as shown in Fig. 8b. Normal mice had the best performance. AD mice with DGLs-PEG-RVG29-D-peptide/pshBACE1-AS NPs treatment showed the most pronounced effect among AD mice with different treatments.

4. Discussion

Herein, for the first time, we have explored the possibility of gene and peptide drug co-delivery across the BBB by brain-targeted drug delivery nanocarriers based on DGLs to treat AD. The rich external amine groups on the surface of DGLs offer plenty reaction sites for functional modifications as well as positive charge for therapeutic gene encapsulation. DGLs offer diverse modes for drug loading including covalent conjugation, electrostatic encapsulation and so on [43,44]. Moreover, the active brain-targeted modification to DGLs renders them the ability to reach the target site by specific binding with receptors or transporters while decreasing the accumulation in non-targeted organs. Based on the above mentioned advantages, DGLs hold great promise as excellent drug delivery nanocarriers for multifunctional drug delivery to treat diseases with complex pathological pathways. In this study, the NPs loading both therapeutic gene and peptide were prepared and characterized successfully (Fig. S1, S2). Though the NPs were slightly positively charged, previous study suggested that nanoparticles with slight positive charge could reach the targeted site following systemic administration [45]. Nanoparticles that were sterically stabilized by PEG modification on their surface and had surface charges that were either slightly negative or slightly positive tend to have minimal self–self and self-non-self interactions [46]. With

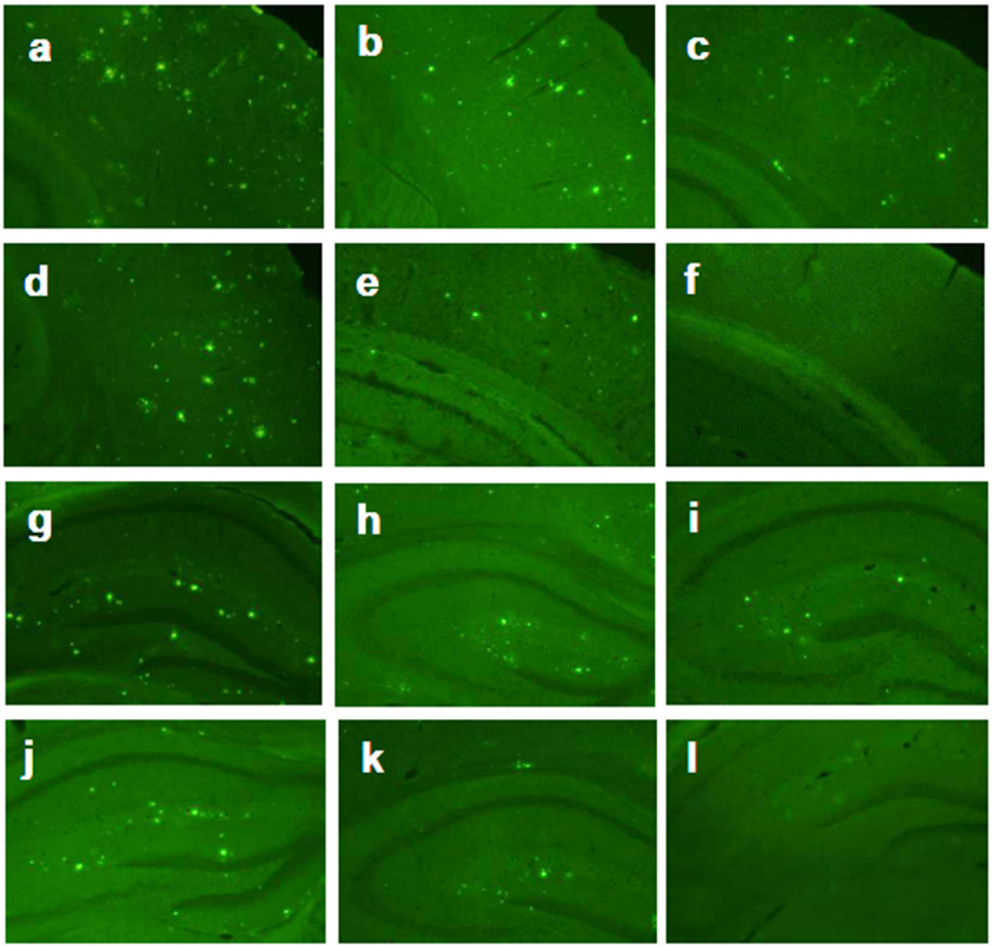

Fig. 6. Thioflavine-S-labeled amyloid plaques distribution. Cortex layer (a–f) and hippocampus (g–l) with different NPs treatments: (a, g) +saline; (b, h) +DGLs-PEG-RVG29/pshSc; (c, i) +DGLs-PEG-RVG29/pshBACE1-AS; (d, j) +DGLs-PEG-RVG29-D-peptide/pshSc; (e, k) +DGLs-PEG-RVG29-D-peptide/pshBACE1-AS; (f, l) non-treated non-transgenic mice. Magnification × 20.

the modification of RVG29, the NPs were able to get across the *in vitro* BBB model more efficiently than the non-targeted NPs (Fig. 3e). The receptors for RVG29 binding are believed to be nicotinic acetylcholine receptor (nACh receptor), which are widely expressed in brain capillary endothelial cells (the main component of BBB) and brain parenchyma cells-like neurons [47]. The cellular uptake of both the therapeutic peptide and gene was significantly higher than that of non-targeted NPs treated group (Fig. 3). The results indicated that DGLs-PEG-RVG29-D-peptide/DNA NPs delivered the peptide and plasmid DNA into the cells simultaneously. The DGLs-PEG-RVG29-D-peptide and DNA dissociated to some extent after uptaken by cells because separated green and red signals were observed in Fig. 3g. The DGLs-PEG-RVG29-D-peptide/DNA NPs were demonstrated to be stable in physiological environment containing serum (Fig. 2e). The dissociation may attribute to amines grafted on the polymer surface with strong proton-absorbing capabilities inside endosomes (pH 5–6) and lysosomes (pH 4–5) after being uptaken, leading to rapid osmotic swelling and DNA release. This dissociation between DGLs component and plasmid DNA is crucial in exerting the synergistic effects of both the peptide and therapeutic gene as their sites of action are located in the cytoplasm and nuclei, respectively. The *in vivo* imaging results also provided convincing evidence that the plasmid and peptide could still be co-delivered efficiently into the brain, despite the uptake of NPs by reticuloendothelial system (RES) organs such as liver and spleen (Fig. 4). The RES uptake was mainly attributed to the nano-scaled size of the drug delivery system [48]. The modification of PEG may reduce the non-specific uptake since PEGylation may help shield the positive charges of DGLs. Thus, the possibility of interactions between NPs and negatively charged membrane during circulation is reduced until the NPs have contact with the specific receptor of RVG29 in BBB. In addition, PEGylation may enable prolonged circulation time by escaping the recognition of immune system [49]. The low immunogenicity of the virus-derived peptide (RVG29) has been proved in previous study [36]. The therapeutic peptide in this study is an all D-type peptide. The D-type peptide is only immunogenic when strong adjuvant is provided. Furthermore, the immune system has preferential recognition of conventional L-peptide [50]. For these reasons, the D-type peptide is less immunogenic than the L-type RVG29 peptide. In support of these claims, the serum interleukin-6 (IL-6), interleukin-1 beta (IL-1β) and tumor necrosis factor-alpha (TNF-α) levels of the NPs treated mice were shown to be similar to the saline treated mice (Fig. S7), demonstrating the low immunogenicity of the NPs. The liver function test result by measuring the serum alanine transaminase (ALT) and aspartate aminotransferase (AST) enzymatic activity (Fig. S8) showed both the enzymatic activity after DGLs-PEG-RVG29-D-peptide/DNA NPs treatment did not change significantly ($p > 0.05$) compared with the saline treated group. As a result, it could be concluded that the NPs did not exert significant

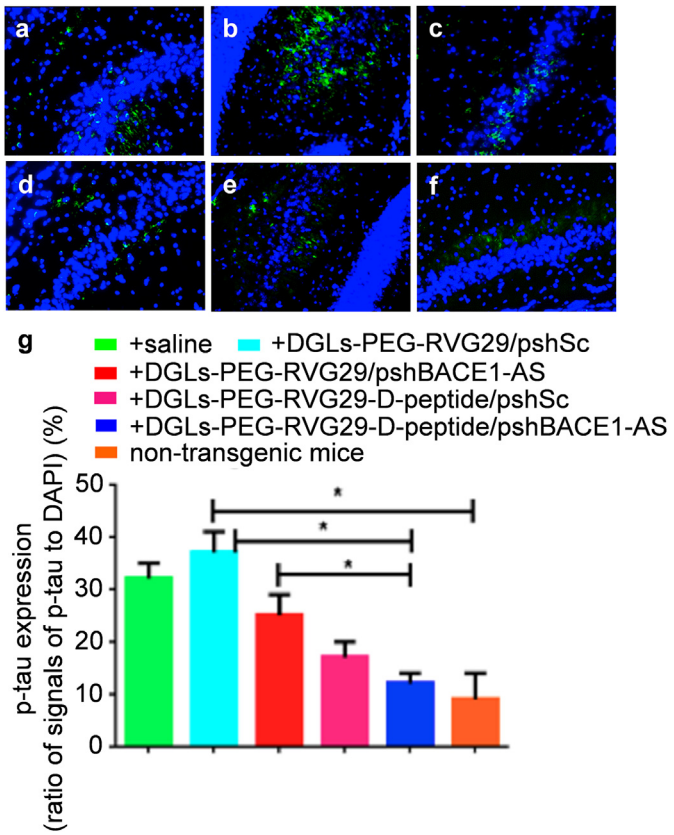

Fig. 7. P-tau positive immunofluorescence indicating the p-tau related fibrils location. (a–f) Hippocampus sections from mice with different NPs treatments: (a) +saline; (b) +DGLs-PEG-RVG29/pshSc; (c) +DGLs-PEG-RVG29/pshBACE1-AS; (d) +DGLs-PEG-RVG29-D-peptide/pshSc; (e) +DGLs-PEG-RVG29-D-peptide/pshBACE1-AS; (f) non-treated non-transgenic mice. Green signal: secondary antibody labeled p-tau antibody. Blue signal: DAPI stained nucleus. Magnification × 20. (g) Quantitative evaluation of p-tau positive immunofluorescence at hippocampus in mice with different NPs treatments. (For interpretation of the references to color in this figure legend, the reader is referred to the web version of this article.)

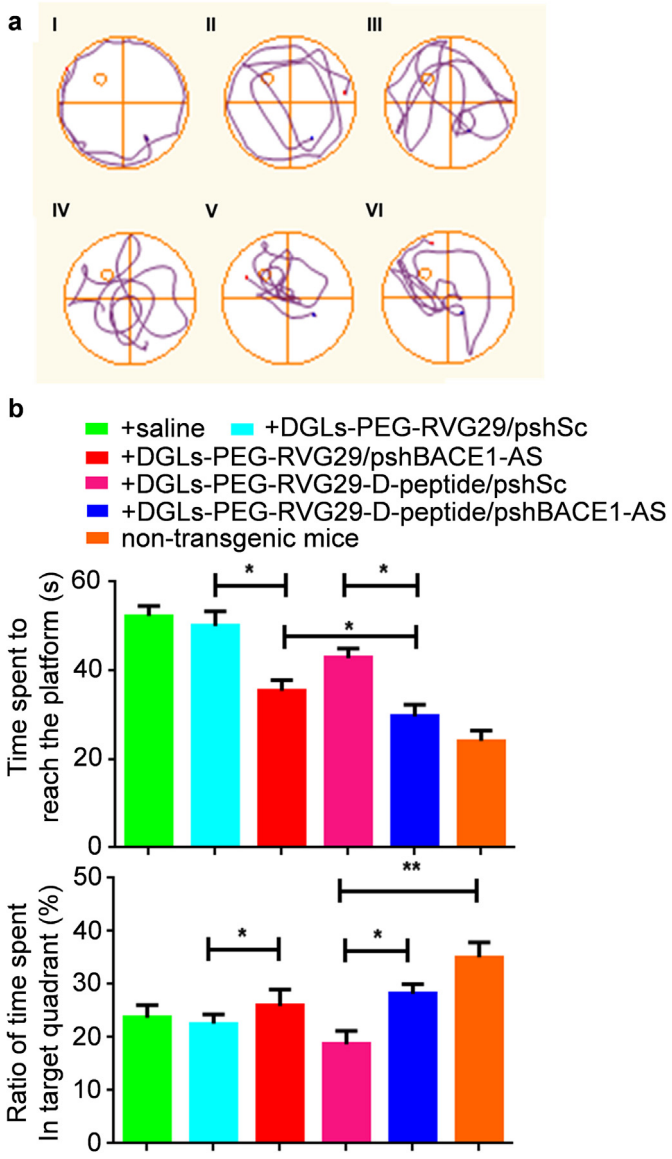

Fig. 8. Morris water maze behavioral evaluation results. (a) Representative swimming path of APP/PS1 mice with different NPs treatment as well as non-transgenic mice. (I) +saline; (II) +DGLs-PEG-RVG29/pshSc; (III) +DGLs-PEG-RVG29/pshBACE1-AS; (IV) +DGLs-PEG-RVG29-D-peptide/pshSc; (V) +DGLs-PEG-RVG29-D-peptide/pshBACE1-AS; (VI) non-treated non-transgenic mice. (b) The average time spent to reach the platform during 1 min (left); Ratio of time spent in target quadrant with 1 min test duration (right). Significance: $^{*}p < 0.05$; $^{**}p < 0.01$, significantly different as compared between two groups.

toxicity to the non-targeted organs such as liver. The renal cells did not have specific uptake pathways for the NPs. They were unlike the BCECs and brain cells that were expressed the specific receptor which could facilitate the NPs through ligand-receptor mediated transcytosis/endocytosis pathways. Previous research showed the nano-scaled drug delivery systems did not caused significant damage to liver and kidney functions [51–53]. As a result, the NPs toxicity in liver and kidney was not supposed as a major issue.

The Aβ deposition and tau hyperphosphorylation are the two main pathological hallmarks in AD. Though the exact molecular mechanism of the interaction between the two pathological pathways remains unclear, the researchers have found the evidence of linking between Aβ and tau pathology. The amyloid-cascade hypothesis stipulates that Aβ is the trigger of all cases of AD and that the tau pathology and other degenerative changes are a downstream consequence of the Aβ pathology [54]. Further studies also suggest that Aβ might trigger or facilitate the accumulation of tau pathology [55]. Abnormal hyperphosphorylation of tau has also been observed in the brains of the APP/PS1 transgenic mice [56]. Another study has also found that intraventricular injection of Infliximab could reduce tau hyperphosphorylation significantly in APP/PS1 transgenic mice [57]. As a result, we have chosen the APP/PS1 transgenic mice as AD model in our study. Yu et al. have reported that compared with age-matched wild-type controls, 9-month-old APP/PS1 double transgenic mice with memory impairment and numerous brain Aβ deposits showed increased numbers of proliferating hippocampal cells [58]. The behavioral changes have been reported to happen when the transgenic mice are 9 months old [59]. Collectively, results indicated that AD progression has a rapid burst in 9 months old APP/PS1 transgenic mice. Thus, in this study, the treatment of therapeutic regimen started at 9 months after birth. It has been shown that the accumulation of Aβ in the brain caused an intriguing combination of aberrant network activity and synaptic depression [60]. β-site APP cleaving enzyme 1 (BACE1) is identified as a major β-secretase in charge of Aβ formation. Researchers also notice that it is important to reduce BACE1 activity, rather than abolish it completely because loss of BACE1 may result in numerous behavioral and physiological deficits including memory loss, emotional deficits, and loss of synaptic

plasticity [31]. Thus, the expression of BACE1 should be regulated precisely allowing the enzyme to perform its physiological functions while avoiding serious consequences of over- or under-expression. A conserved noncoding antisense transcript for BACE1 (BACE1-AS) can rapidly up-regulate BACE1 levels in response to a variety of stresses such as $A\beta_{1-42}$ exposure. BACE1-AS could increase the stability of BACE1 mRNA. As a result, the down-regulation of BACE1-AS can reduce the BACE1 activity in an indirect manner, avoiding extreme reduction in BACE1 level. Treatment with BACE1-AS RNA interference (RNAi) may achieve a preferential reduction of stress-induced increase in BACE1 expression without disturbing physiologically basal expression levels. The shRNA-encoding plasmid was used in this study because it was thought to be more stable than siRNA or shRNA for *in vivo* applications [9]. In our previous study, we have successfully demonstrated the efficient *in vitro* and *in vivo* reporter gene expression such as red fluorescence protein and luciferase by delivering the plasmids using DGLs [61,62]. In Fig. 5, the transcript of BACE1-AS was found to be lower in AD mice treated with the NPs loading BACE1-AS shRNA-encoding plasmid with/without modification of therapeutic peptide. It was also observed that the level of BACE1-AS RNA transcript was elevated compared to non-transgenic mice. The down-regulation of BACE1-AS, in turn, lowered the BACE1 mRNA levels. The BACE1 mRNA in transgenic mice was also found to be higher than that of normal mice. The reduction of BACE1 level was also confirmed. Knowing that the reduction of BACE1 level leads to the decrease of Aβ formation as BACE1 is a crucial enzyme in the process of APP cleavage to Aβ, amyloid deposition staining has been performed. The staining revealed less deposition in mice brain treated with the NPs loading BACE1-AS shRNA-encoding plasmid with/without modification of therapeutic peptide (Fig. 6 and Fig. S6). The change of amyloid deposition staining was in accordance to that of BACE1 level. This result also demonstrated that the BACE1 level affects the Aβ deposition.

The intracellular fibrils are believed to be as another main characteristic of AD. Thus, inhibition of p-tau-related fibril formation would provide an effective strategy to prevent or delay the progress of AD. Sievers et al. showed that computer-aided, structure-based design could yield highly specific peptide inhibitors of fibrils formation [38]. Using known atomic structures of segments of fibrils as templates, an all-D-amino-acid inhibitor (sequence: D-TLKIVW, named as D-peptide) was designed and characterized to disrupt the p-tau-associated fibril formation in AD. With the addition of brain-targeted NPs platform, this therapeutic peptide was delivered into the brain and moderately inhibited the fibril formation as shown in p-tau specific immunostaining (Fig. 7).

Progressive memory loss and cognitive dysfunction are the hallmark clinical features of Alzheimer's disease (AD) [19]. Because the amyloid and neurofibrillary pathology are predominantly confined to the hippocampus and cortex, learning and memory could be evaluated using the Morris water maze [63–65]. The Aβ deposition in amygdala area in the current APP/PS1 mice model which could induce neuropsychiatric symptoms was reported to appear from 11 to 17 months old [66]. As a result, the neuropsychiatric parameters such as anxiety, depression and stress were not be able to evaluate since we started the treatment from 9 months old. The behavioral results from the Morris water maze test showed the pharmacodynamics of the NPs treatment (Fig. 8). The best therapeutic effect was observed in AD mice treated with NPs loading BACE1-AS shRNA-encoding plasmid and therapeutic peptide. The result suggested that the reduction of Aβ deposition and inhibition of p-tau associated fibril both contributed to block the progression of AD behavioral manifestations. Using the multifunctional drug delivery system, the synergistic effect from both the peptide and gene was conducive to the therapeutic effects in AD. When combined the results of Fig. 8 in single therapeutic component (either therapeutic peptide or gene) loaded NPs treated groups, it was worth mentioning that the performance of AD mice treated with DGLs-PEG-RVG29/pshBACE1-AS NPs was better than that treated with DGLs-PEG-RVG29-D-peptide/pshSc NPs. Whether reduction of Aβ burden was a more efficient therapeutic target than inhibition of p-tau related fibril is still worth exploring as there are some limitations in the present study design. Firstly, the regimen was designed based on the Aβ formation timeline given that the studies on fibril formation in transgenic AD mice were insufficient. The treatment start point and interval could be further optimized when progress of the disease is further explored. By the nanoparticles reported in this study, the BACE1 level could be fine-regulated according to the progress of the diseases because of the transient regulation feature of non-viral gene delivery system. Specifically, if the disease progress is deteriorated, the dose of the therapeutic plasmid could be increased. If the disease progress is decelerated, the interval of injection could be elongated. Secondly, the doses of therapeutic gene and peptide may need to be further optimized in large-scale pharmacodynamics evaluation. The DGLs was able to condense completely with DNA at the weight ratio ranging from 2:1 to 10:1 (DGLs/DNA, w/w). As there were 123 amine groups on the surface of the DGLs, the PEGylation could be further increased to load more peptides. Thirdly, due the instinct feature of nano-scaled delivery system and concrete structure of the BBB, the ratio of NPs transcytosis across the BBB need to be improved by rational design of the NPs system based on more understanding about the nanomedicine and the BBB in the future. It would be more challenging to achieve the precise targeted delivery in sub-organ areas such as hippocampus, the most affected area in AD to maximum the therapeutic effects of the NPs.

5. Conclusions

In this study, a multifunctional nanocarrier for therapeutic gene and peptide co-delivery based on DGLs with brain-targeted modification has been successfully developed for AD treatment. Reduction of Aβ plaque deposition and inhibition of p-tau-related fibril formation have been chosen as dual therapeutic targets. The therapeutic gene and peptide drug for the two therapeutic targets are co-delivered efficiently across the BBB and into the brain utilizing the brain-targeted DGLs NPs through different drug loading modes. A multiple-dosing regimen is designed by considering the progressive and long-term characteristics of AD, as well as taking advantages of high biocompatibility and degradability of DGLs. A series of mechanism investigation and pharmacodynamics evaluation have demonstrate simultaneous efficacy of gene therapy targeting the BACE1 noncoding RNA in concert with peptide therapy targeting the p-tau related fibril formation. In the future, the nanocarriers will be further optimized by tuning the ratio of drug loading or screening targeting modification to achieve better efficacy. In addition, the multifunctional nanocarriers based on DGLs also hold great promise for treatment of other diseases with complex pathological pathways with rational design.

Competing financial interests

The authors declare no competing financial interests.

Acknowledgments

This work was supported by the grant from National Science Fund for Distinguished Young Scholars (81425023) and National Natural Science Foundation of China (81172993). The authors thanked Pro. Jianhua Zhu (School of Pharmacy, Fudan University)

for the radiolabeled work. The authors thanked Kenya Nagasaka (Department of Materials Science and Engineering, University of Illinois at Urbana-Champaign) for the grammar and spelling check.

Appendix A. Supplementary data

Supplementary data related to this article can be found at http://dx.doi.org/10.1016/j.biomaterials.2015.11.060.

References

[1] T. Sun, Y.S. Zhang, B. Pang, D.C. Hyun, M. Yang, Y. Xia, Engineered nanoparticles for drug delivery in cancer therapy, Angew. Chem. Int. Ed. Engl. 53 (2014) 12320–12364.
[2] W. Jiang, B.Y. Kim, J.T. Rutka, W.C. Chan, Advances and challenges of nanotechnology-based drug delivery systems, Expert Opin. Drug Deliv. 4 (2007) 621–633.
[3] Y. Wang, L. Miao, A. Satterlee, L. Huang, Delivery of oligonucleotides with lipid nanoparticles, Adv. Drug Deliv. Rev. (2015) 68–80.
[4] X. Gu, H. Chen, X. Gao, Nanotherapeutic strategies for the treatment of Alzheimer's disease, Ther. Deliv. 6 (2015) 177–195.
[5] L.M. Ittner, J. Gotz, Amyloid-beta and tau–a toxic pas de deux in Alzheimer's disease, Nat. Rev. Neurosci. 12 (2011) 65–72.
[6] C. Ballatore, V.M. Lee, J.Q. Trojanowski, Tau-mediated neurodegeneration in Alzheimer's disease and related disorders, Nat. Rev. Neurosci. 8 (2007) 663–672.
[7] E. Karran, M. Mercken, B. De Strooper, The amyloid cascade hypothesis for Alzheimer's disease: an appraisal for the development of therapeutics, Nat. Rev. Drug Discov. 10 (2011) 698–712.
[8] W.M. Pardridge, Blood-brain barrier delivery, Drug Discov. Today 12 (2007) 54–61.
[9] R. Pahuja, K. Seth, A. Shukla, R.K. Shukla, P. Bhatnagar, L.K. Chauhan, P.N. Saxena, J. Arun, B.P. Chaudhari, D.K. Patel, S.P. Singh, R. Shukla, V.K. Khanna, P. Kumar, R.K. Chaturvedi, K.C. Gupta, Trans-blood brain barrier delivery of dopamine loaded nanoparticles reverses functional deficits in Parkinsonian rats, ACS Nano (2015) 4850–4871.
[10] B. Angelov, A. Angelova, M. Drechsler, V.M. Garamus, R. Mutafchieva, S. Lesieur, Identification of large channels in cationic PEGylated cubosome nanoparticles by synchrotron radiation SAXS and Cryo-TEM imaging, Soft Matter 11 (2015) 3686–3692.
[11] A. Angelova, B. Angelov, M. Drechsler, S. Lesieur, Neurotrophin delivery using nanotechnology, Drug Discov. Today 18 (2013) 1263–1271.
[12] B. Angelov, A. Angelova, S.K. Filippov, T. Narayanan, M. Drechsler, P. Stepanek, P. Couvreur, S. Lesieur, DNA/fusogenic lipid nanocarrier assembly: millisecond structural dynamics, J. Phys. Chem. Lett. 4 (2013) 1959–1964.
[13] B. Angelov, A. Angelova, S.K. Filippov, M. Drechsler, P. Stepanek, S. Lesieur, Multicompartment lipid cubic nanoparticles with high protein upload: millisecond dynamics of formation, ACS Nano 8 (2014) 5216–5226.
[14] A. Angelova, B. Angelov, M. Drechsler, V.M. Garamus, S. Lesieur, Protein entrapment in PEGylated lipid nanoparticles, Int. J. Pharm. 454 (2013) 625–632.
[15] C. Geral, A. Angelova, S. Lesieur, From molecular to nanotechnology strategies for delivery of neurotrophins: emphasis on brain-derived neurotrophic factor (BDNF), Pharmaceutics 5 (2013) 127–167.
[16] A. Angelova, B. Angelov, R. Mutafchieva, S. Lesieur, P. Couvreur, Self-assembled multicompartment liquid crystalline lipid carriers for protein, peptide, and nucleic acid drug delivery, Acc. Chem. Res. 44 (2011) 147–156.
[17] L. Miao, S. Guo, J. Zhang, W.Y. Kim, L. Huang, Nanoparticles with precise ratiometric co-loading and co-delivery of gemcitabine monophosphate and cisplatin for treatment of bladder cancer, Adv. Funct. Mater. 24 (2014) 6601–6611.
[18] S. Guo, C.M. Lin, Z. Xu, L. Miao, Y. Wang, L. Huang, Co-delivery of cisplatin and rapamycin for enhanced anticancer therapy through synergistic effects and microenvironment modulation, ACS Nano 8 (2014) 4996–5009.
[19] L.M. Billings, S. Oddo, K.N. Green, J.L. McGaugh, F.M. LaFerla, Intraneuronal Abeta causes the onset of early Alzheimer's disease-related cognitive deficits in transgenic mice, Neuron 45 (2005) 675–688.
[20] L.M. Ittner, Y.D. Ke, F. Delerue, M. Bi, A. Gladbach, J. van Eersel, H. Wolfing, B.C. Chieng, M.J. Christie, I.A. Napier, A. Eckert, M. Staufenbiel, E. Hardeman, J. Gotz, Dendritic function of tau mediates amyloid-beta toxicity in Alzheimer's disease mouse models, Cell 142 (2010) 387–397.
[21] E.D. Roberson, K. Scearce-Levie, J.J. Palop, F. Yan, I.H. Cheng, T. Wu, H. Gerstein, G.Q. Yu, L. Mucke, Reducing endogenous tau ameliorates amyloid beta-induced deficits in an Alzheimer's disease mouse model, Science 316 (2007) 750–754.
[22] R.W. Choy, Z. Cheng, R. Schekman, Amyloid precursor protein (APP) traffics from the cell surface via endosomes for amyloid beta (Abeta) production in the trans-golgi network, Proc. Natl. Acad. Sci. U. S. A. 109 (2012) E2077–E2082.
[23] R.J. O'Brien, P.C. Wong, Amyloid precursor protein processing and Alzheimer's disease, Annu. Rev. Neurosci. 34 (2011) 185–204.
[24] E.B. Lee, B. Zhang, K. Liu, E.A. Greenbaum, R.W. Doms, J.Q. Trojanowski, V.M. Lee, BACE overexpression alters the subcellular processing of APP and inhibits Abeta deposition in vivo, J. Cell Biol. 168 (2005) 291–302.
[25] Y. Jiang, K.A. Mullaney, C.M. Peterhoff, S. Che, S.D. Schmidt, A. Boyer-Boiteau, S.D. Ginsberg, A.M. Cataldo, P.M. Mathews, R.A. Nixon, Alzheimer's-related endosome dysfunction in down syndrome is Abeta-independent but requires APP and is reversed by BACE-1 inhibition, Proc. Natl. Acad. Sci. U. S. A. 107 (2010) 1630–1635.
[26] I. Hussain, J. Hawkins, D. Harrison, C. Hille, G. Wayne, L. Cutler, T. Buck, D. Walter, E. Demont, C. Howes, A. Naylor, P. Jeffrey, M.I. Gonzalez, C. Dingwall, A. Michel, S. Redshaw, J.B. Davis, Oral administration of a potent and selective non-peptidic BACE-1 inhibitor decreases beta-cleavage of amyloid precursor protein and amyloid-beta production in vivo, J. Neurochem. 100 (2007) 802–809.
[27] O. Singer, R.A. Marr, E. Rockenstein, L. Crews, N.G. Coufal, F.H. Gage, I.M. Verma, E. Masliah, Targeting BACE1 with siRNAs ameliorates Alzheimer disease neuropathology in a transgenic model, Nat. Neurosci. 8 (2005) 1343–1349.
[28] G. Evin, A. Barakat, C.L. Masters, BACE: therapeutic target and potential biomarker for Alzheimer's disease, Int. J. Biochem. Cell Biol. 42 (2010) 1923–1926.
[29] H. Ma, S. Lesne, L. Kotilinek, J.V. Steidl-Nichols, M. Sherman, L. Younkin, S. Younkin, C. Forster, N. Sergeant, A. Delacourte, R. Vassar, M. Citron, P. Kofuji, L.M. Boland, K.H. Ashe, Involvement of beta-site APP cleaving enzyme 1 (BACE1) in amyloid precursor protein-mediated enhancement of memory and activity-dependent synaptic plasticity, Proc. Natl. Acad. Sci. U. S. A. 104 (2007) 8167–8172.
[30] F.M. Laird, H. Cai, A.V. Savonenko, M.H. Farah, K. He, T. Melnikova, H. Wen, H.C. Chiang, G. Xu, V.E. Koliatsos, D.R. Borchelt, D.L. Price, H.K. Lee, P.C. Wong, BACE1, a major determinant of selective vulnerability of the brain to amyloid-beta amyloidogenesis, is essential for cognitive, emotional, and synaptic functions, J. Neurosci. 25 (2005) 11693–11709.
[31] M.A. Faghihi, F. Modarresi, A.M. Khalil, D.E. Wood, B.G. Sahagan, T.E. Morgan, C.E. Finch, G. St Laurent 3rd, P.J. Kenny, C. Wahlestedt, Expression of a non-coding RNA is elevated in Alzheimer's disease and drives rapid feed-forward regulation of beta-secretase, Nat. Med. 14 (2008) 723–730.
[32] Y. Gao, L. Chen, Z. Zhang, Y. Chen, Y. Li, Reversal of multidrug resistance by reduction-sensitive linear cationic click polymer/iMDR1-pDNA complex nanoparticles, Biomaterials 32 (2011) 1738–1747.
[33] K.R. Brunden, J.Q. Trojanowski, V.M. Lee, Advances in tau-focused drug discovery for Alzheimer's disease and related tauopathies, Nat. Rev. Drug Discov. 8 (2009) 783–793.
[34] F.G. De Felice, D. Wu, M.P. Lambert, S.J. Fernandez, P.T. Velasco, P.N. Lacor, E.H. Bigio, J. Jerecic, P.J. Acton, P.J. Shughrue, E. Chen-Dodson, G.G. Kinney, W.L. Klein, Alzheimer's disease-type neuronal tau hyperphosphorylation induced by A beta oligomers, Neurobiol. Aging 29 (2008) 1334–1347.
[35] S.A. Sievers, J. Karanicolas, H.W. Chang, A. Zhao, L. Jiang, O. Zirafi, J.T. Stevens, J. Münch, D. Baker, D. Eisenberg, Structure-based design of non-natural amino-acid inhibitors of amyloid fibril formation, Nature 475 (2011) 96–100.
[36] P. Kumar, H. Wu, J.L. McBride, K.E. Jung, M.H. Kim, B.L. Davidson, S.K. Lee, P. Shankar, N. Manjunath, Transvascular delivery of small interfering RNA to the central nervous system, Nature 448 (2007) 39–43.
[37] Y. Liu, R. Huang, L. Han, W. Ke, K. Shao, L. Ye, J. Lou, C. Jiang, Brain-targeting gene delivery and cellular internalization mechanisms for modified rabies virus glycoprotein RVG29 nanoparticles, Biomaterials 30 (2009) 4195–4202.
[38] H. Cottet, M. Martin, A. Papillaud, E. Souaid, H. Collet, A. Commeyras, Determination of dendrigraft poly-L-lysine diffusion coefficients by taylor dispersion analysis, Biomacromolecules 8 (2007) 3235–3243.
[39] I. Tsogas, T. Theodossiou, Z. Sideratou, C.M. Paleos, H. Collet, J.C. Rossi, B. Romestand, A. Commeyras, Interaction and transport of poly(L-lysine) dendrigrafts through liposomal and cellular membranes: the role of generation and surface functionalization, Biomacromolecules 8 (2007) 3263–3270.
[40] Y. Xie, L. Ye, X. Zhang, W. Cui, J. Lou, T. Nagai, X. Hou, Transport of nerve growth factor encapsulated into liposomes across the blood-brain barrier: in vitro and in vivo studies, J. Control Release 105 (2005) 106–119.
[41] D.L. Ridley, J. Pakkanen, S. Wonnacott, Effects of chronic drug treatments on increases in intracellular calcium mediated by nicotinic acetylcholine receptors in SH-SY5Y cells, Br. J. Pharmacol. 135 (2002) 1051–1059.
[42] R.J. Lukas, S.A. Norman, L. Lucero, Characterization of nicotinic acetylcholine receptors expressed by cells of the SH-SY5Y human neuroblastoma clonal line, Mol. Cell Neurosci. 4 (1993) 1–12.
[43] Y. Kuang, S. An, Y. Guo, S. Huang, K. Shao, Y. Liu, J. Li, H. Ma, C. Jiang, T7 peptide-functionalized nanoparticles utilizing RNA interference for glioma dual targeting, Int. J. Pharm. 454 (2013) 11–20.
[44] T. Liu, F. Oukacine, H. Collet, A. Commeyras, L. Vial, H. Cottet, Monitoring surface functionalization of dendrigraft poly-L-lysines via click chemistry by capillary electrophoresis and Taylor dispersion analysis, J. Chromatogr. A 1273 (2013) 111–116.
[45] S. Hu-Lieskovan, J.D. Heidel, D.W. Bartlett, M.E. Davis, T.J. Triche, Sequence-specific knockdown of EWS-FLI1 by targeted, nonviral delivery of small interfering RNA inhibits tumor growth in a murine model of metastatic Ewing's sarcoma, Cancer Res. 65 (2005) 8984–8992.
[46] M.E. Davis, Z.G. Chen, D.M. Shin, Nanoparticle therapeutics: an emerging treatment modality for cancer, Nat. Rev. Drug Discov. 7 (2008) 771–782.
[47] M.O. Oyewumi, R.A. Yokel, M. Jay, T. Coakley, R.J. Mumper, Comparison of cell

uptake, biodistribution and tumor retention of folate-coated and PEG-coated gadolinium nanoparticles in tumor-bearing mice, J. Control Release 95 (2004) 613–626.
[48] S.H. Kim, J.H. Jeong, K.W. Chun, T.G. Park, Target-specific cellular uptake of PLGA nanoparticles coated with poly(L-lysine)-poly(ethylene glycol)-folate conjugate, Langmuir 21 (2005) 8852–8857.
[49] S.D. Li, L. Huang, Stealth nanoparticles: high density but sheddable PEG is a key for tumor targeting, J. Control Release 145 (2010) 178–181.
[50] P. Chong, C. Sia, B. Tripet, O. James, M. Klein, Comparative immunological properties of enantiomeric peptides, Lett. Pept. Sci. 3 (1996) 99–106.
[51] L. Liu, K. Xu, H. Wang, P.K. Tan, W. Fan, S.S. Venkatraman, L. Li, Y.Y. Yang, Self-assembled cationic peptide nanoparticles as an efficient antimicrobial agent, Nat. Nanotechnol. 4 (2009) 457–463.
[52] V. Pokharkar, S. Dhar, D. Bhumkar, V. Mali, S. Bodhankar, B.L. Prasad, Acute and subacute toxicity studies of chitosan reduced gold nanoparticles: a novel carrier for therapeutic agents, J. Biomed. Nanotechnol. 5 (2009) 233–239.
[53] C.H. Hou, S.M. Hou, Y.S. Hsueh, J. Lin, H.C. Wu, F.H. Lin, The in vivo performance of biomagnetic hydroxyapatite nanoparticles in cancer hyperthermia therapy, Biomaterials 30 (2009) 3956–3960.
[54] J. Hardy, D.J. Selkoe, The amyloid hypothesis of Alzheimer's disease: progress and problems on the road to therapeutics, Science 297 (2002) 353–356.
[55] S. Oddo, A. Caccamo, J.D. Shepherd, M.P. Murphy, T.E. Golde, R. Kayed, R. Metherate, M.P. Mattson, Y. Akbari, F.M. LaFerla, Triple-transgenic model of Alzheimer's disease with plaques and tangles: intracellular Abeta and synaptic dysfunction, Neuron 39 (2003) 409–421.
[56] M.A. Kurt, D.C. Davies, M. Kidd, K. Duff, D.R. Howlett, Hyperphosphorylated tau and paired helical filament-like structures in the brains of mice carrying mutant amyloid precursor protein and mutant presenilin-1 transgenes, Neurobiol. Dis. 14 (2003) 89–97.
[57] J.Q. Shi, W. Shen, J. Chen, B.R. Wang, L.L. Zhong, Y.W. Zhu, H.Q. Zhu, Q.Q. Zhang, Y.D. Zhang, J. Xu, Anti-TNF-alpha reduces amyloid plaques and tau phosphorylation and induces CD11c-positive dendritic-like cell in the APP/PS1 transgenic mouse brains, Brain Res. 1368 (2011) 239–247.
[58] Y. Yu, J. He, Y. Zhang, H. Luo, S. Zhu, Y. Yang, T. Zhao, J. Wu, Y. Huang, J. Kong, Q. Tan, X.M. Li, Increased hippocampal neurogenesis in the progressive stage of Alzheimer's disease phenotype in an APP/PS1 double transgenic mouse model, Hippocampus 19 (2009) 1247–1253.
[59] P.E. Cramer, J.R. Cirrito, D.W. Wesson, C.Y. Lee, J.C. Karlo, A.E. Zinn, B.T. Casali, J.L. Restivo, W.D. Goebel, M.J. James, K.R. Brunden, D.A. Wilson, G.E. Landreth, ApoE-directed therapeutics rapidly clear beta-amyloid and reverse deficits in AD mouse models, Science 335 (2012) 1503–1506.
[60] Y. Huang, L. Mucke, Alzheimer mechanisms and therapeutic strategies, Cell 148 (2012) 1204–1222.
[61] R. Huang, S. Liu, K. Shao, L. Han, W. Ke, Y. Liu, J. Li, S. Huang, C. Jiang, Evaluation and mechanism studies of PEGylated dendrigraft poly-L-lysines as novel gene delivery vectors, Nanotechnology 21 (2010) 265101.
[62] Y. Liu, J. Li, K. Shao, R. Huang, L. Ye, J. Lou, C. Jiang, A leptin derived 30-amino-acid peptide modified pegylated poly-L-lysine dendrigraft for brain targeted gene delivery, Biomaterials 31 (2010) 5246–5257.
[63] R.J. Sutherland, R.J. McDonald, Hippocampus, amygdala, and memory deficits in rats, Behav. Brain Res. 37 (1990) 57–79.
[64] K.H. Ashe, Learning and memory in transgenic mice modeling Alzheimer's disease, Learn Mem. 8 (2001) 301–308.
[65] C. Janus, J. Pearson, J. McLaurin, P.M. Mathews, Y. Jiang, S.D. Schmidt, M.A. Chishti, P. Horne, D. Heslin, J. French, H.T. Mount, R.A. Nixon, M. Mercken, C. Bergeron, P.E. Fraser, P. St George-Hyslop, D. Westaway, A beta peptide immunization reduces behavioural impairment and plaques in a model of Alzheimer's disease, Nature 408 (2000) 979–982.
[66] P.J. Pistell, M. Zhu, D.K. Ingram, Acquisition of conditioned taste aversion is impaired in the amyloid precursor protein/presenilin 1 mouse model of Alzheimer's disease, Neuroscience 152 (2008) 594–600.